Long term seismicity monitoring of the Rittershoffen deep geothermal reservoir

Rike Koepke[12], Olivier Lengliné[2], Emmanuel Gaucher[1], Jean Schmittbuhl[2], Thomas Kohl[1]

[1]Geothermal Research/AGW, Karlsruhe Institute of Technology, Kaiserstr. 12, 76131 Karlsruhe, Germany

[2] IPGS/EOST, University of Strasbourg/CNRS, 5 rue René Descartes, 67084 Strasbourg, France

rike.koepke@kit.edu

Keywords: Induced seismicity, Template matching, Deep geothermal reservoir characterization

ABSTRACT

The seismicity induced during the development of the deep geothermal reservoir of Rittershoffen (Alsace, France) was monitored continuously by an extensive seismic network of up to 43 stations. We apply a template matching algorithm to the continuous seismic waveforms recorded during the thermal and hydraulic stimulations of the GRT1 well and during the drilling of the GRT2 well to get a robust seismic database for reservoir characterization. As templates, we use a manually repicked seismic catalogue covering these three periods. We relocate the detected seismic events with HypoDD to get precise relative locations. This work presents an overview of the temporal and spatial development of the induced seismicity during the different operations in the reservoir and gives insight into the geometry of the underground structures.

1. INTRODUCTION

In a geothermal reservoir, seismicity may be induced due to pressure changes in the underground as a result of drilling, stimulation or circulation operations (Cuenot et al., 2008; Pearson, 1981). The induced seismic events are therefore strongly linked to the fluid flow and the geological structures that make this fluid flow possible. Hence, induced seismicity can be a powerful tool to get insight into the underground fracture network and to characterize the architecture and the flow processes in the reservoir (Deichmann et al., 2014; Michelet and Toksöz, 2007). Unlike drill-cores and well-logs that provide a direct but very local image of the reservoir, induced seismicity has the potential to highlight structures farther away from the wells. Yet, the interpretation of induced seismicity clouds as a fracture and fault system is challenging and requires an extensive database. This means, on the one hand, that the detection of as many earthquakes as possible belonging to the relevant structures would be desirable and, on the other hand, that the locations of these earthquakes have to be determined precisely and accurately.

Conventional STA/LTA detectors for seismic event detection from continuous waveforms only detect events with relatively high signal-to-noise ratio (Earle and Shearer, 1994). The database is thus usually limited by the magnitudes of the events and the noise obscuring the waveforms. Therefore, we want to apply a template matching algorithm in this study. This technique outperforms STA/LTA detectors in terms of sensitivity to events with low signal-to-noise ratio and picking consistency for events with waveforms similar to the chosen templates. Examples for the successful application of template matching include various contexts like the detection of aftershocks (Peng and Zhao, 2009), basal sliding of glaciers (Helmstetter et al., 2015), volcano dynamics (Lengliné et al., 2016) and induced seismicity (Huang and Beroza, 2015; Skoumal et al., 2014).

We want to apply the technique to the seismicity induced in the Rittershoffen deep geothermal reservoir. While Lengliné et al. (2017) focused solely on the hydraulic stimulation of the well GRT1, here we cover the thermal and hydraulic stimulation of GRT1 and the drilling of the well GRT2 to observe the development of the reservoir during the different stages. With the template matching approach, new events with waveforms similar to the templates can be detected. The technique is therefore particularly suitable to find earthquake clusters. This is an important aspect of the reservoir characterization, since such clusters can image main geological structures. The objective of this study is to identify such structures and comprehend their evolution during the development of the Rittershoffen reservoir.

In the following, we first give an overview about the Rittershoffen deep geothermal reservoir and present the database, which is the basis for this study. Then we describe the template matching algorithm we use and the parameter settings we chose to apply. Finally, we present the temporal and spatial distribution of the induced seismicity and give an overview of the structures we detected in the reservoir.

2. DATABASE

The Rittershoffen deep geothermal reservoir is located in the Upper Rhine Valley (Alsace, France) close to the EGS plant of Soultz-sous-Forêts. The characteristics and development of the site are described in detail in Baujard et al. (2017). The first well, GRT1, was drilled from September to December 2012, the second well,

GRT2, from May to July 2014. The well doublet targets a fault zone in the 2.5 km deep reservoir just beneath the transition from the sedimentary cover to the granitic basement. Hot brine of about 170°C is extracted and used to supply 24 MWt to a nearby bio-refinery (Baujard et al., 2017).

GRT1 showed a low initial productivity of about 0.45 L/s/bar at the nominal flowrate of 70 L/s. To increase the productivity the well underwent first a thermal stimulation from the 23th to 25th of April 2013. A total volume of 4,230 m^3 water with a temperature of 12°C was injected with injection rates ranging from 10 L/s to 25 L/s. From June 23rd to 25th the well was stimulated chemically and directly afterwards, on the 27th and 28th of June, a hydraulic stimulation took place with injection rates of up to 80 L/s. After the stimulation operations, the final injectivity index of the well reached about 2.5 L/s/bar. The well GRT2 was not stimulated because the natural productivity was already high enough with 2.8-3.5 L/s/bar (Baujard et al., 2017).

The seismicity induced during the development of the reservoir was monitored continuously by different seismic networks presented in Maurer et al. (2005). The permanent seismic network monitoring the Rittershoffen and the Soutz geothermal sites is composed of 12 surface stations. Additionally, 16 temporary surface stations were installed in June 2013 but only some of them were already in operation during the hydraulic stimulation of GRT1. Before the drilling of GRT2, another 15 temporary stations were added. The seismic events induced during thermal and hydraulic stimulation of GRT1 and drilling of GRT2 have been repicked manually, resulting in a catalogue of over 1300 events, which we use as a template database (Maurer et al., submitted).

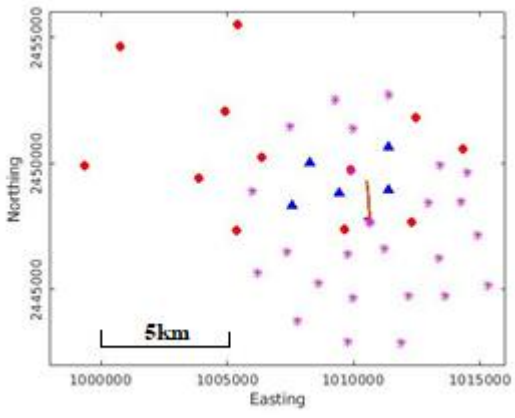

Figure 1: Seismic networks active during thermal stimulation of GRT1 (red circles), hydraulic stimulation of GRT1 (additional blue triangles) and drilling of GRT2 (additional magenta stars). Orange line: wellpath GRT2, black line: wellpath GRT1 (nearly vertical). Coordinates in Lambert II etendu (m).

For the first period, the thermal stimulation of GRT1, the template database contains 146 events recorded on the 24th and 25th of April, 2013. At this time only the 12 permanent station with in total 26 channels where deployed (Fig. 1, red circles). During the second period, the hydraulic stimulation of GRT1, the network consisted of 17 stations in operation with in total 41 channels (Fig. 1, red circles and blue triangles). The template database for this period contains 990 events and covers the time period from the 27th of June to the 4th of July, 2013. During the third period, the drilling of GRT2, 184 events have been detected and manually repicked, all occurring on the 26th of April 2014. At this time, the network consisted of 43 operating stations with 119 channels (Fig. 1, all symbols).

3. TEMPLATE MATCHING

To obtain a robust database for the reservoir characterization, we applied a template matching algorithm to the continuous waveforms recorded by the seismic networks. This technique is based on the calculation of the correlation coefficient between continuous and template waveforms. Thus, we use a known seismic signal (template) to detect new events with similar waveforms but with signal to noise ratios even lower than 1, which is not possible with conventional STA/LTA detectors. Since only events similar to the templates will be detected, an important choice to make is on the composition of the template database.

There are different approaches to build the template database, like dividing the potential templates in clusters of similar waveforms and choosing or calculating one template representative for each cluster. These approaches have the advantage to save computation time and to limit double-detections, which have to be found and eliminated later. On the other hand, events, which are not similar enough to the cluster representative but would have been detected by one of its members, may be missed. Our goal in this study is to obtain a database as complete as possible and computation time is not a deciding factor. Therefore, we used all manually repicked events in the catalogue as templates, but as three distinct databases for each period. The template windows are 2.56 s long and start 0.5 s before the P-wave pick.

All continuous waveforms and template waveforms are re-sampled to 100 Hz and filtered by a band-pass filter between 10 and 45 Hz to optimize the signal-to-noise ration. The band-pass filter range has been chosen by comparative power spectral density analysis of the template signals and the continuous signal of one day. We chose the 25 channels, which have been picked most frequently on the templates and sorted them from most to the least picks. Correlation is computed every 0.01 s for the first six of these 25 channels where a pick on the template is available.

After the computation of the correlation coefficients on these six channels for a given template, the correlation vectors are time-shifted according to the travel-time differences between the stations computed for the template. Then, maximum filtering (Gil and Werman, 1993; van Herk, 1992) over a duration of 0.1 s is

applied on each channel before the channels are stacked and a mean correlation coefficient is calculated. If the mean correlation coefficient exceeds a certain threshold, a new event is considered to be detected. If multiple templates detect the same event, it is associated with the template that detects it with the highest correlation coefficient.

We tested the described template matching algorithm on a sample of the Rittershoffen dataset to find a suitable threshold for the correlation coefficient above which a new event is considered to be detected. To do this, we calculated the distribution of correlation coefficients over a whole day of detection for several different templates and channels. The distribution of the correlation coefficient proved to be very different for the different cases, so we concluded that a fixed threshold would not be sufficient. We want to apply an objective threshold in order to achieve a selected false alarm rate adapted to each specific case. Therefore, this threshold should take into account the given template, the quality of the signal at each station where the detection is performed and the network quality.

To achieve that, we implemented a case adaptive threshold similar to the approach proposed by Slinkard et al. (2014). We calculate for each template a time- and polarity-shifted version, which has the advantage that it keeps the same time-bandwidth product as the original data and the same number of independent samples. We run the detection algorithm on these subverted templates and calculate the detection statistics. Since the waveforms of the subverted templates have characteristics similar to the real templates, yet completely artificial, we assume that they should not be correlated to the continuous waveforms. Under this null hypothesis, we can compute the threshold necessary to achieve a desired false alarm rate independently for each template and for each day of the continuous waveforms.

We apply the described template matching algorithm to the 3 periods introduced above. For all detections, we extract the seismic waveforms 0.5 s before the P-wave arrival over a duration of 2.56 s on all channels for which the template that detected the event had been picked.

3. RELOCATION

After detection, we relocate the events with the Software HypoDD (Waldhauser and Ellsworth, 2000). HypoDD uses a double-difference algorithm and allows the calculation of precise relative locations between events with similar waveforms. As input, we calculate the travel time differences on all available channels between all detected events. For the relocation, we keep only travel time differences of event pairs computed with a correlation coefficient higher than 0.5 on, at least, six channels. This ensures that the relation of an event pair is stable and prevents that the locations of outliers are taken too much into account. The initial locations of the events for relocation are set on the wellpath of GRT1 at 2300 m depth, where hydraulic injection occurred.

For relocation, we use a 1D velocity model created from VSP-measurements and three-component sonic logging conducted in GRT1. It is the same model used by Kinnaert et al. (2016) to conduct earthquake location error modelling for the Rittershoffen site. The velocity model consists of 13 layers, including 3 low-velocity layers. P-wave velocity ranges from 1318 m/s to 5815 m/s, Vp/Vs-ratio from 1.68 to 2.12 with an average of 1.9 down to 2.3 km.

4. TEMPORAL DISTRIBUTION OF THE INDUCED SEISMICITY

With the template matching algorithm we detected 299 events for the thermal stimulation of GRT1, 2959 events for the hydraulic stimulation of GRT1 and 300 events for the drilling of GRT2. Hence, the event database for period 1 was doubled, for period 2 nearly tripled and for period 3 increased by half. Table 2 shows the distribution of events per day in the template databases and of the newly detected events. Like already described by Maurer et al. (2015), it is apparent that period 2 actually consists of two intervals of seismic activity separated by a quiet period. The first burst of activity is directly correlated with the injection period of the hydraulic stimulation, whereas the second burst of seismicity occurred 4 days after shut-in. During the quiet period in-between, only 6 events had been previously picked, now 32 have been detected.

Table 1: Amount/Distribution of induced seismic events manually picked and detected by template matching.

Day	Manually picked	Template matching
Period 1: Thermal stimulation GRT1		
24.04.2013	66	179
25.04.2013	80	120
Period 2: Hydraulic stimulation GRT1		
27.06.2013	515	1263
28.06.2013	310	1198
29.06.2013	0	2
30.06.2013	5	14
01.07.2013	1	13
02.07.2013	154	439
03.07.2013	2	20
04.07.2013	3	10
Period 3: Drilling GRT2		
26.04.2014	184	300

Figure 2 shows the distribution of seismic events over time for all three periods. The number of events is summed over time bins of one hour. Baujard et al. (2017) describe the thermal and hydraulic stimulation of GRT1 in detail, which allows us to relate the

temporal development of the seismicity during these periods to the injection flowrate.

The injection of cold water during the thermal stimulation started already on the 23rd of April with a flowrate of 10 L/s, but induced seismicity only started when the injection flowrate was increased to 20 L/s on the 24th of April. The seismicity rate reached its peak, with about 55 events per hour, when the flowrate was increased to 25 L/s in the night from the 24th to the 25th of April, then decreased while the flowrate still remained constant and went to zero half a day before shut-in.

During the hydraulic stimulation the flowrate has been increased stepwise form zero on the 27th of June at 11:20 to 80 L/s on the 28th of June early morning and then stepwise decreased again till shut-in at 9:00. The automatic detections implied that the seismicity started only after the flow rate was increased to 40 L/s (Baujard et al., 2017), however, our database shows that seismicity started a little earlier, when the flowrate was increased to about 25 L/s, which was the flowrate previously reached during the thermal stimulation. The seismicity rate then increased with the increasing flowrate to about 450 events per hour and then decreased immediately when the flowrate was decreased.

Directly after the hydraulic stimulation an injection test was performed on the 28th of June from 11:00 to 17:30. The flowrate did not exceed 60 L/s and nearly no seismicity was detected. Thus, the seismicity occurrence during the hydraulic stimulation highlights a Kaiser effect in two instances. Right at the start of the operation seismicity was observed only once the flow rate reached the highest level of the previous injection rate during the thermal stimulation. During the subsequent injection test, which did not reach the maximum flowrate of the stimulation, nearly no seismicity occurred.

After the hydraulic stimulation, the site remained seismically quiet for about four days. Then, a short seismicity burst occurred with over 400 events in not much more than an hour. No injection, production or circulation operations were performed at this time, which could have induced this seismic activity. It is therefore most likely related to the hydraulic stimulation and the subsequent injection test.

The induced seismicity that occurred during the drilling of GRT2 was also temporally very concentrated. All monitored seismicity occurred on one day, the 26th of April, nearly exclusively in a time interval of two hours.

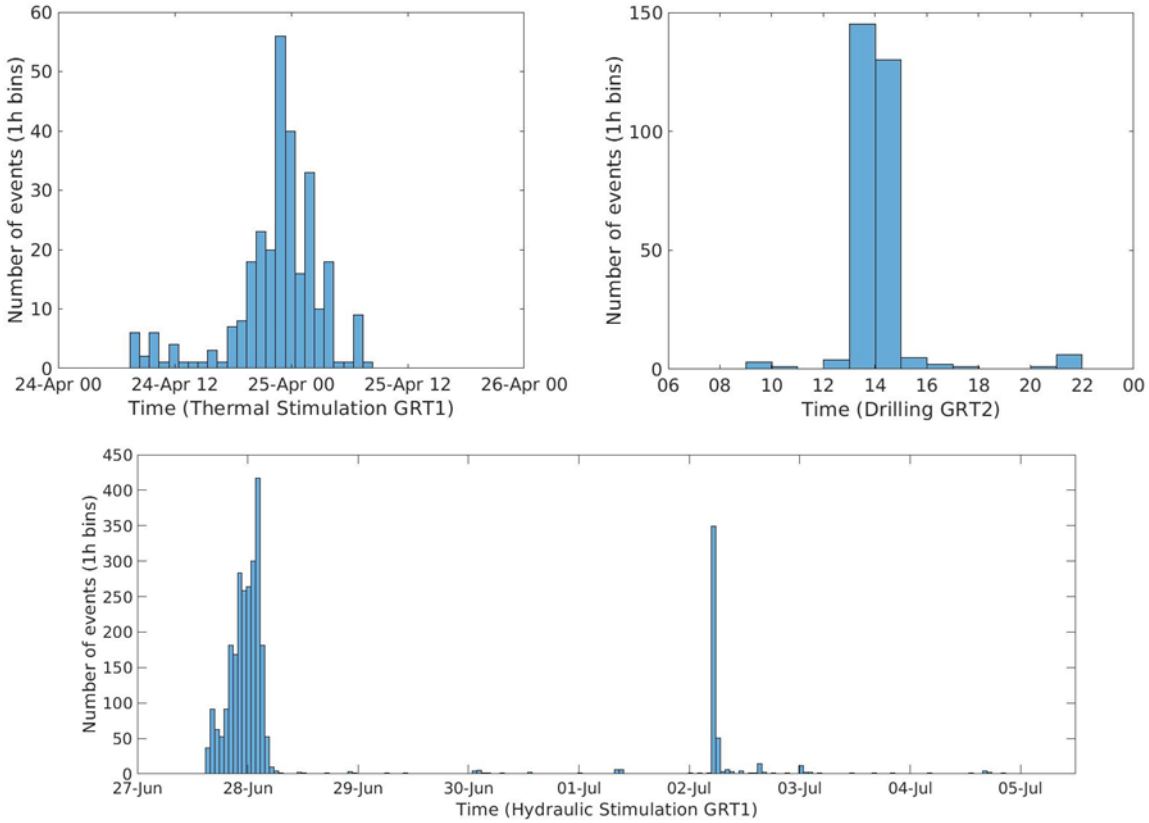

Figure 2: Distribution of induced seismicity with time for the thermal stimulation of GRT1 (top left, time as date and hours), the hydraulic stimulation of GRT1 (bottom) and drilling of GRT2 (top right, time as hours on the 26th of April 2014). Hourly rate of earthquake is represented as blue vertical bars.

5. SPATIAL DISTRIBUTION OF THE INDUCED SEISMICITY

While we applied the template matching algorithm for detection to all 3 periods separately, we relocate them together to ensure that the three seismic clouds have reliable relative locations towards each other. Among the 3558 detected events in total, we could relocate 3112 events under the constraints we applied. 210 events are relocated for period 1, 2641 events for period 2 and 261 events for period 3.

The development of the seismicity over all three periods is shown in Figure 3. During the thermal stimulation, the induced seismicity develops SSW from the well and downward, and forms a quite localized, quasi-planar structure (Fig. 3, red cloud). The same part of the reservoir is also seismically active during the hydraulic stimulation, but the seismicity extends farther south and covers overall a wider area (Fig. 3, blue cloud). The same geological structure is activated during both stimulations. A small proportion of the seismic events induced during the hydraulic stimulation is located further north and isolated from the main cloud.

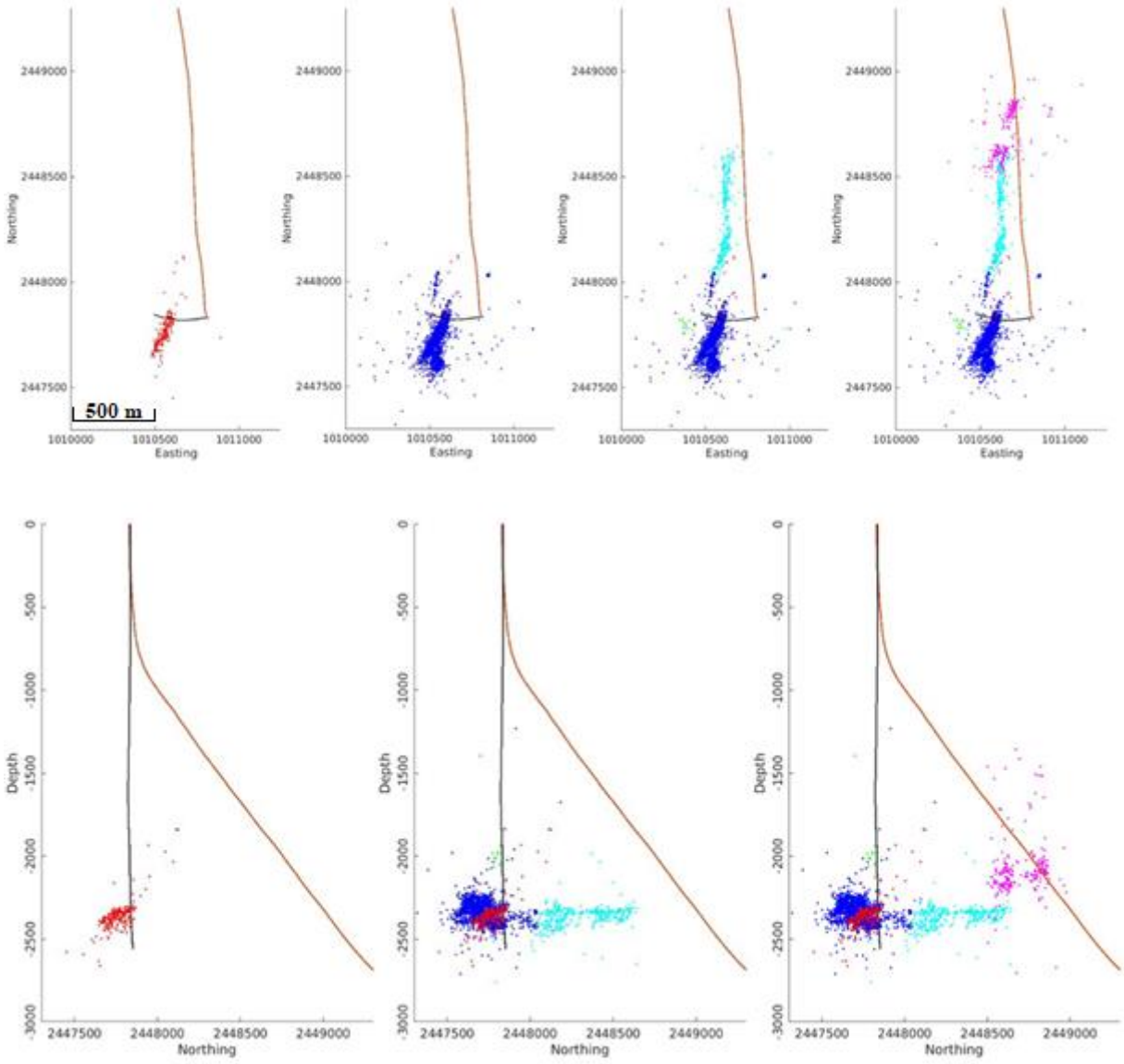

Figure 3: Spatial distribution of induced seismicity for the thermal stimulation of GRT1 (red), hydraulic stimulation of GRT1 (blue), the subsequent quiet period (green) and seismicity burst (cyan) and drilling of GRT2 (magenta). Black line: wellpath GRT1, orange line: wellpath GRT2. Coordinates in Lambert II etendu (m).

This isolated part of the cloud is connected to the seismicity induced during the short burst 4 days after the hydraulic stimulation (Fig. 3, cyan cloud). The seismicity of this time interval develops north on an elongated structure that changes its orientation slightly from nearly N in the part that was already active during the hydraulic stimulation to NNE and back to N. The north-depth cross section shows, that the structure advances nearly horizontally northwards towards GRT2 without much shift in depth. We observe that it is shifted compared to the fault activated during the hydraulic stimulation and evidences an en échelon system.

In the map view, we see that the seismicity induced during the drilling of GRT2 (Fig. 3, magenta cloud) proceeds northward on the same elongated structure, now again orientated more NNE. However, the north-depth section shows, that there is an offset in depth of nearly 150 m between the seismicity of period 2 and period 3. Additionally, the seismicity induced during the drilling forms two distinct clusters, which seem to be aligned but separated from each other. One is located at the edge of the elongated structure, the other directly on the GRT2-wellpath.

To summarize, there seem to be at least two, maybe three different structures activated in the reservoir during the three periods we examined. The first structure intersects GRT1 in the open hole section and is activated during the thermal and the hydraulic stimulation of GRT1. It has been described by Lengliné et al. (2017) by a best fitting plane striking N025° E and dipping 74° towards west, which agrees with our observations. The second structure is located farther north and more elongated in shape. It is characterized by a slightly varying orientation changing from N to NNE to N to NNE from its southern to its northern edge. The seismicity induced during the drilling of GRT2 appears to be located on this second structure, although there is an offset in depth, which may indicate a third structure with similar orientation. Also, seismicity during the drilling is concentrated in two separated clusters which may or may not belong to the same geological structure.

When interpreting the induced seismicity clouds as reservoir structures, one has to keep in mind that the relocation in HypoDD is foremost giving relative locations. The absolute positions of the clusters may well be different. Indeed, relocation attempts with different initial locations for the earthquakes has shown that not only the position but also the size of the detected structures can vary greatly. Furthermore, the geology of the reservoir is quite complex due to the presence of different lithological layers and a major fault. This complexity is unlikely to be well represented by a 1D velocity model. The study of Kinnaert et al. (2016) shows, that neglecting the major fault in the Rittershoffen reservoir and the associated shift of the lithological layers introduces a strong location bias of several hundred meters. Therefore, the question remains whether some of the shifts and offsets between the clusters we observed are associated with real geological features or are artefacts due to the limits of the relocation approach we used.

6. CONCLUSION AND OUTLOOK

We applied a template matching algorithm to the seismicity induced at Rittershoffen during thermal stimulation of the GRT1 well, hydraulic stimulation of GRT1 including the subsequent quiet period and seismicity burst, and the drilling of the GRT2 well. In total, we nearly tripled the amount of seismic events by this procedure while being least effective for the drilling of GRT2, where the amount of events have been only increased by half. The occurrence of seismicity put in relation with the flow rate during the stimulation of GRT1 revealed a clear Kaiser effect. It could be observed at the beginning of the hydraulic stimulation when the seismicity started only after the flow rate reached the maximum flowrate from the thermal stimulation and during the injection test that followed the hydraulic stimulation where no seismicity was observed.

We then relocated the detected events to use their locations to image the seismically active structures in the reservoir. During the thermal stimulation and the hydraulic stimulation, the same NNE-oriented structure has been activated close to the well GRT1. During the seismic burst following the hydraulic stimulation, a second structure became active, located farther north with an offset to the first structure and a varying orientation between NNE and N. It stretches horizontally towards GRT2. During the drilling of GRT2, the seismicity occurred in two separated clusters, which match the orientation of the northern structure but show an offset in depth and between each other.

As next steps, we want to confirm our results by applying other relocation procedures. We want to relocate the events in a 3D velocity model and better constrain the absolute relocations by using non-linear approaches for relocation. Furthermore, in this study we used as templates only events from one operational period at a time. Since it seems that the structures activated during the different periods may have some connection to each other, we want to use the templates from all periods to detect new events during each period. This may further enhance our database. We also want to apply a clustering analysis concerning waveform similarity to better understand the relations of the structures in the induced seismic clouds.

REFERENCES

Baujard, C., Genter, A., Dalmais, E., Maurer, V., Hehn, R., Rosillette, R., Vidal, J. and Schmittbuhl, J.: Hydrothermal characterization of wells GRT-1 and GRT-2 in Rittershoffen, France: Implications on the understanding of natural flow systems in the rhine graben, *Geothermics*, 65, (2017), 255–268.

Cuenot, N., Dorbath, C. and Dorbath, L.: Analysis of the Microseismicity Induced by Fluid Injections at the EGS Site of Soultz-sous-Forêts (Alsace,

France): Implications for the Characterization of the Geothermal Reservoir Properties, *Pure Appl. Geophys.*, 165, (2008), 797–828.

Deichmann, N., Kraft, T. and Evans, K.F.: Identification of faults activated during the stimulation of the Basel geothermal project from cluster analysis and focal mechanisms of the larger magnitude events, *Geothermics*, 52, (2014), 84–97.

Earle, P.S. and Shearer, P.M.: Characterization of global seismograms using an automatic-picking algorithm, *Bull. Seismol. Soc. Am.*, 84, (1994), 366–376.

Gil, J. and Werman, M.: Computing 2-D Min, Median, and Max Filters, *IEEE Trans. Pattern Anal. Mach. Intell.*, 15, (1993), 504–507.

Helmstetter, A., Nicolas, B., Comon, P. and Gay, M.: Basal icequakes recorded beneath an Alpine glacier (Glacier d'Argentière, Mont Blanc, France): Evidence for stick-slip motion?, *J. Geophys. Res. Earth Surf*, 120, (2015), 379–401.

Huang, Y. and Beroza, G.C.: Temporal variation in the magnitude-frequency distribution during the Guy-Greenbrier earthquake sequence: Variation in MFD for Induced Seismicity, *Geophys. Res. Lett.*, 42, (2015), 6639–6646.

Kinnaert, X., Gaucher, E., Achauer, U. and Kohl, T.: Modelling earthquake location errors at a reservoir scale: a case study in the Upper Rhine Graben, *Geophys. J. Int.*, 206, (2016), 861–879.

Lengliné, O., Boubacar, M. and Schmittbuhl, J.: Seismicity related to the hydraulic stimulation of GRT1, Rittershoffen, France, *Geophys. J. Int.*, 208, (2017), 1704-1715.

Lengliné, O., Duputel, Z. and Ferrazzini, V.: Uncovering the hidden signature of a magmatic recharge at Piton de la Fournaise volcano using small earthquakes, *Geophys. Res. Lett.*, 43, (2016), 4255–4262.

Lomax, A., Virieux, J., Volant, P. and Berge-Thierry, C.: Probabilistic Earthquake Location in 3D and Layered Models, in: Advances in Seismic Event Location, Modern Approaches in Geophysics, Thurber, C.H., Rabinowitz, N. (Ed.), 101-134, *Springer Netherlands*, Dordrecht, (2000).

Maurer, V., Cuenot, N., Gaucher, E., Grunberg, M., Vergne, J., Wodling, H., Lehujeur, M. and Schmittbuhl, J.: Seismic Monitoring of the Rittershoffen EGS Project (Alsace, France), *Proceedings of the World Geothermal Congress 2015*, Melbourne, Australia, (2015).

Maurer, V., Gaucher, E., Grunberg, M., Koepke, R. and Pestourie, R.: Seismicity induced during the development of the Rittershoffen geothermal field, France. (submitted).

Michelet, S. and Toksöz, M.N.: Fracture mapping in the Soultz-sous-Forêts geothermal field using microearthquake locations, *J. Geophys. Res*, 112, (2007).

Pearson, C.: The relationship between microseismicity and high pore pressures during hydraulic stimulation experiments in low permeability granitic rocks, *J. Geophys. Res. Solid Earth*, 86, (1981), 7855–7864.

Peng, Z. and Zhao, P.: Migration of early aftershocks following the 2004 Parkfield earthquake, *Nat. Geosci.*, 2, (2009), 877–881.

Skoumal, R.J., Brudzinski, M.R., Currie, B.S. and Levy, J.: Optimizing multi-station earthquake template matching through re-examination of the Youngstown, Ohio, sequence, *Earth Planet. Sci. Lett.*, 405, (2014), 274–280.

Slinkard, M., Schaff, D., Mikhailova, N., Heck, S., Young, C. and Richards, P.G.: Multistation Validation of Waveform Correlation Techniques as Applied to Broad Regional Monitoring, *Bull. Seismol. Soc. Am.*, 104, (2014), 2768–2781.

van Herk, M.: A fast algorithm for local minimum and maximum filters on rectangular and octagonal kernels, *Pattern Recognit. Lett.*, 13, (1992), 517–521.

Waldhauser, F. and Ellsworth, W.L.: A Double-Difference Earthquake Location Algorithm: Method and Application to the Northern Hayward Fault, California, *Bull. Seismol. Soc. Am.*, 90, (2000), 1353–1368.

Acknowledgements

The authors thank the ECOGI joint venture and the Electricité de Strasbourg – Géothermie (ES-G) company for sharing seismological and operational data. The Geophysical Instrument Pool Potsdam, from the GFZ German Research Centre for Geosciences, provided the temporary seismological units of the monitoring network. The deployment of the temporary network was conducted and partly funded within the frame of the excellence laboratory "LabEx G-EAU-THERMIE PROFONDE" (University of Strasbourg) as part of the French "Investments for the future" of the French National Research Agency. We also thank V. Maurer, M. Grunberg, N. Cuenot and R. Pestourie for their work on the seismological database we took as reference.